Journal of Sound and Vibration (2000) **233**(2), 255–277
doi:10.1006/jsvi.1999.2797, available online at http://www.idealibrary.com on IDEAL®

PROPELLER NOISE FIELDS

M. CARLEY

Department of Mechanical and Manufacturing Engineering, Trinity College, Dublin 2, Ireland

(*Received* 14 *July* 1999, *and in final form* 18 *November* 1999)

An efficient method is derived for the calculation of the acoustic field of a rotating source. The technique is used to study the effect of variations in loading and thickness distributions on the noise radiated by subsonic and supersonic propellers in forward flight. Results are compared with previously published asymptotic analyses and are found to be accurate.

1. INTRODUCTION

The sound field radiated by rotating systems such as propellers and helicopter rotors has a rich structure, displaying a wide range of complex behaviour. This complexity makes the study of such systems both scientifically challenging and technologically important. Rotating systems are widely used for aircraft propulsion and the environmental implications of farfield noise and structural effects in the nearfield mean that the acoustics of such systems are important in the design and operation of most aircraft. At the same time, the complexity of such systems means that predicting the radiated acoustic field and its underlying physical behaviour is not a trivial task. Propeller noise has been of interest for almost as long as there have been aeroplanes with work on its theoretical prediction dating back to at least 1919 [1]. Since then, the studies of Gutin [2] and of Garrick and Watkins [3] have been important advances in the field. It is the work of Lighthill [4], however, which forms the basis of modern aeroacoustics and of present methods for the prediction of noise from aircraft powerplant. The developments of that theory which are used in acoustical calculations for solid bodies [5, 6] have been reworked for improved numerical implementation, the methods of Farassat and co-workers [7, 8] and of Hanson [9] being the most important in this regard.

The main methods of propeller noise prediction, however, are "single-point" techniques. They provide a means of predicting the noise at one point at a time. Even with high-speed computing facilities, they do not allow the detailed investigation of the properties of the acoustic field around a realistic rotating source. The principal reason for this is the number of points at which the field must be calculated if its structure is to be adequately resolved. For any serious investigation, the field must be resolved at scales much shorter than one acoustic wavelength. For a modern high-speed rotor, this is an extremely demanding task.

For this reason, a large number of approximate methods have been developed, many of them based on asymptotic analysis [10–12]. These give results which retain most of the accuracy of full numerical evaluation of the acoustic integrals but require much less computation. Furthermore, they also indicate explicitly the dependence of the acoustic field on flight and source parameters. For example, in the far field it can be shown that the blade tip dominates the noise of subsonic rotors [10] while the Mach radius dominates supersonic rotor noise [11]. Such analyses yield information about the physics of the system which

0022-460X/00/220255 + 23 $35.00/0

would be difficult to obtain in any other manner and have proven extremely useful both scientifically and technologically.

Another development, which forms the basis of the work presented here, has been the study of exact solutions of model problems which contain the essential details of the real system. In particular, the work of Chapman on the sound field of supersonic rotors [13] and on the properties of the Green's function for the noise radiated by a rotating source [14] have demonstrated the richness of structure possessed by the acoustic field of spinning sources. In a later paper [15], Chapman presents a novel method for the fast, exact, numerical calculation of the field radiated by certain classes of rotating source distributions. The method reduces the two-dimensional acoustic integral to a one-dimensional integral, using a co-ordinate transformation. The restrictions on the approach are that it applies only to a stationary propeller of even blade number and that the source strength on the blades does not vary with radius. The method has since been extended by Carley [16] to include forward motion and odd blade number. The purpose of the present paper is to extend the method to include arbitrary source distributions and hence to make the method suitable for industrial applications as well as for the study of the general properties of the acoustic field of rotating sources.

2. ACOUSTIC MODEL

A method exists for the efficient numerical calculation of the sound field of a rotating source when the source distribution is independent of source radius [15, 16]. In this section, it is shown how this work can be related to the general problem of a propeller of arbitrary source distribution. The standard acoustic integrals are first derived and then manipulated into a form suitable for application of the previously developed method. The system to be studied is shown in Figure 1. A propeller of radius a rotating at angular velocity Ω operates

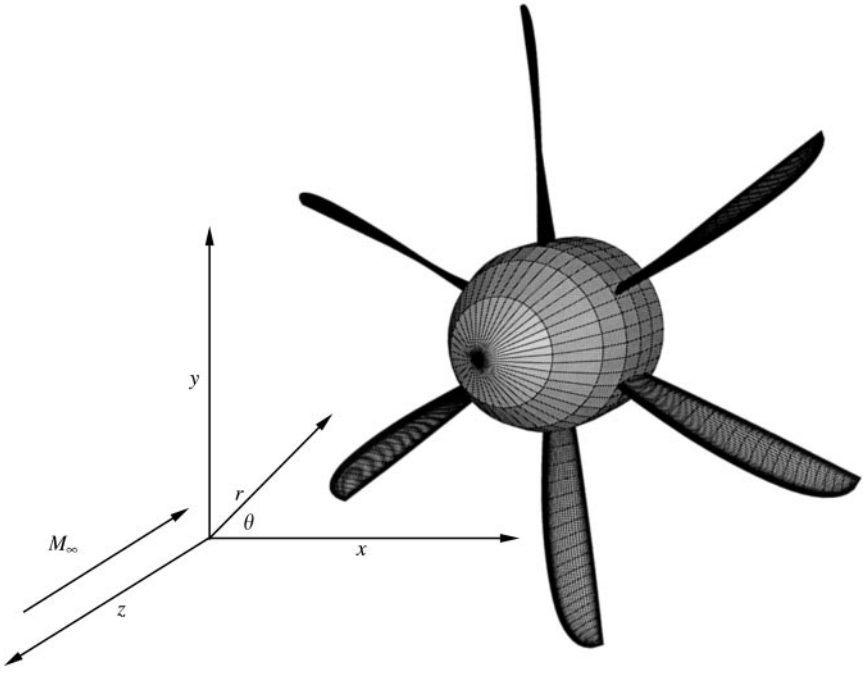

Figure 1. Propeller noise model and co-ordinates

at a flight Mach number M_∞. Co-ordinates are chosen so that the propeller translates in the positive z direction or is stationary in a mean flow in the negative z direction. In both cases, the observer is stationary. Cylindrical co-ordinates (r, θ, z) are used. The blade geometry and surface pressure distributions give rise to "thickness" and "loading" noise respectively. Since the source terms are periodic, they can be decomposed into Fourier series in blade azimuth with the nth term contributing $s_n(r_1)\exp[jn(\theta_1 - \Omega t)]$ where the propeller co-ordinates are (r_1, θ_1). Given the Fourier coefficients corresponding to the operating conditions and propeller geometry, the problem of calculating the acoustic field then reduces to the evaluation of a set of integrals over the propeller disc. The fundamental theory for the radiated noise is that of Goldstein [6]:

$$p_T = \frac{\mathrm{D}}{\mathrm{D}t}\int_{-\infty}^{\infty}\int_{A(\tau)}\frac{\rho v_n}{4\pi S}\delta(t-\tau-\sigma/c)\,\mathrm{d}A\,\mathrm{d}\tau \quad \text{(thickness)}, \tag{1a}$$

$$p_L = -\nabla.\int_{-\infty}^{\infty}\int_{A(\tau)}\frac{\mathbf{F}}{4\pi S}\delta(t-\tau-\sigma/c)\,\mathrm{d}A\,\mathrm{d}\tau \quad \text{(loading)}, \tag{1b}$$

where A is the surface of the source, in this case the propeller disc, τ is the emission time of the sound reaching the observer at time t, v_n is the surface normal velocity and $\mathbf{F}$ is the force applied to the fluid. The fluid density and speed of sound are ρ and c respectively.

The Green's function is that given by Garrick and Watkins [3]:

$$G(\mathbf{x}, t; \mathbf{y}, \tau) = \frac{\delta(t-\tau-\sigma/c)}{4\pi S}. \tag{2}$$

In the frequency domain, for a source with time dependence $\exp(-j\omega t)$

$$G = \frac{\mathrm{e}^{jk\sigma}}{4\pi S}, \qquad k = \omega/c. \tag{3}$$

The phase and amplitude radii σ and S depend on the case being considered. For a translating propeller, co-ordinates are chosen such that its axial displacement is $z = cM_\infty t$:

$$S = [\beta^2(r^2 + r_1^2 - 2rr_1\cos(\theta - \theta_1)) + (z - cM_\infty t)^2]^{1/2}, \tag{4a}$$

$$\sigma = (S + M_\infty z)/\beta^2, \tag{4b}$$

$$\beta^2 = (1 - M_\infty^2).$$

When the propeller and observer are stationary in a uniform flow

$$S = [\beta^2(r^2 + r_1^2 - 2rr_1\cos(\theta - \theta_1)) + z^2]^{1/2}, \tag{5a}$$

$$\sigma = (S + M_\infty z)/\beta^2 \tag{5b}$$

with the propeller disc lying in the plane $z = 0$.

The time derivative D/Dt is

$$\frac{\mathrm{D}}{\mathrm{D}t} = \begin{cases} \partial/\partial t & \text{stationary fluid,} \\ \partial/\partial t - M_\infty \partial/\partial z & \text{moving fluid.} \end{cases}$$

Inserting the source definitions into equation (1) and using the shifting property of the Dirac delta to perform the integration in τ, the noise due to the nth harmonic of thickness and loading is

$$p_T = -\mathrm{j}n\Omega\rho \frac{\mathrm{D}}{\mathrm{D}t} \int_{a_0}^{a} \int_0^{2\pi} \frac{\mathrm{e}^{\mathrm{j}(k\sigma - n\Omega t - n\theta_1)}}{4\pi S} h_n(r_1) r_1 \,\mathrm{d}\theta_1 \,\mathrm{d}r_1, \tag{6a}$$

$$p_L = -\nabla \cdot \int_{a_0}^{a} \int_0^{2\pi} \frac{\mathrm{e}^{\mathrm{j}(k\sigma - n\Omega t - n\theta_1)}}{4\pi S} \mathbf{F}_n(r_1) r_1 \,\mathrm{d}\theta_1 \,\mathrm{d}r_1. \tag{6b}$$

Here h_n is the nth harmonic of the propeller blade geometry, with $-\mathrm{j}n\Omega h_n \exp(-\mathrm{j}n\Omega t)$ the velocity perturbation. The rotor hub of radius a_0 is assumed to generate no noise.

Non-dimensionalizing the problem so that pressure is scaled on ρc^2, length on a and velocity on c:

$$p_\mathrm{T} = -n^2 M_t^2 \mathrm{e}^{\mathrm{j}n\theta} I(r, \theta, z, n, M_t, M_\infty),$$

$$I = \int_0^{2\pi} \int_{r_0}^{1} h_n(r_1) \frac{\mathrm{e}^{\mathrm{j}(k\sigma - n\theta_1)}}{4\pi S^3} \left(S\sigma + \mathrm{j} \frac{M_\infty}{M_t} \frac{z}{n} \right) r_1 \,\mathrm{d}r_1 \,\mathrm{d}\theta_1, \tag{7a}$$

$$p_\mathrm{L} = \mathrm{e}^{\mathrm{j}n\theta} L(r, \theta, z, n, M_t, M_\infty) - \mathrm{j}n\mathrm{e}^{\mathrm{j}n\theta} Q(r, \theta, z, n, M_t, M_\infty),$$

$$L = \int_0^{2\pi} \int_{r_0}^{1} g_n(r_1) \frac{\mathrm{e}^{\mathrm{j}(k\sigma - n\theta_1)}}{4\pi S^3} \left(z - \mathrm{j} \frac{kS}{\beta^2} (z + M_\infty S) \right) r_1 \,\mathrm{d}r_1 \,\mathrm{d}\theta_1, \tag{7b}$$

$$Q = \frac{1}{r} \int_0^{2\pi} \int_{r_0}^{1} q_n(r_1) \frac{\mathrm{e}^{\mathrm{j}(k\sigma - n\theta_1)}}{4\pi S} r_1 \,\mathrm{d}r_1 \,\mathrm{d}\theta_1 \tag{7c}$$

and

$$S = [\beta^2(r^2 + r_1^2 - 2rr_1 \cos\theta_1) + (z - cM_\infty t)^2]^{1/2} \quad \text{(stationary fluid)},$$

$$S = [\beta^2(r^2 + r_1^2 - 2rr_1 \cos\theta_1) + z^2]^{1/2} \quad \text{(moving fluid)}.$$

Here r_0 is the non-dimensional hub radius. The force $\mathbf{F}_n$ has been decomposed into thrust and drag terms g_n and q_n, respectively, radial forces being neglected. The blade tip rotational Mach number is $M_t = \Omega a/c$ and the acoustic wavenumber $k = nM_t$. These results are the complex conjugates of equations (21) and (23) of Garrick and Watkins' report [3].

2.1. CALCULATION OF THE ACOUSTIC FIELD

The problem to be dealt with now is that of efficiently evaluating the integrals of equation (7) to allow the acoustic field to be studied in detail. The objective is the exact calculation of

I, L and Q in a large enough field and at sufficiently fine resolution to show the structure of the acoustic field. This means that the field must be calculated on a mesh with a characteristic size of considerably less than one acoustic wavelength. The method which is chosen must also be efficient enough to allow the field to be evaluated sufficiently quickly to permit parametric studies to be conducted in a reasonable time. Such a method has been developed previously for a restricted subproblem of that which is addressed here and the purpose of this section is to show how it can be used in evaluating the acoustic integrals of equation (7).

Only the thickness noise integral I is examined for the moment, L and Q being treated by an analogous method. First, a new integral I_c is defined:

$$I_c(r_1) = \int_0^{2\pi} \int_0^{r_1} \frac{e^{j(k\sigma - n\theta_1)}}{4\pi S^3} \left(S\sigma + j \frac{M_\infty}{M_t} \frac{z}{n} \right) r_1' \, dr_1' \, d\theta_1, \quad 0 \leqslant r_1 \leqslant 1. \tag{8}$$

This is the sound radiated by a sub-disc of radius r_1 with $h_n \equiv 1$. Differentiating with respect to r_1

$$\frac{dI_c}{dr_1} = \int_0^{2\pi} \frac{e^{j(k\sigma - n\theta_1)}}{4\pi S^3} \left(S\sigma + j \frac{M_\infty}{M_t} \frac{z}{n} \right) r_1 \, d\theta_1.$$

Recognizing the θ_1-integral of equation (7a), I can be rewritten as

$$I = \int_{r_0}^{1} h_n(r_1) \frac{dI_c}{dr_1} dr_1$$

and integrating by parts

$$I = h_n(1) I_c(1) - h_n(r_0) I_c(r_0) - \int_{r_0}^{1} \frac{dh_n}{dr_1} I_c(r_1) \, dr_1. \tag{9}$$

Finally, it is noted that

$$I_c(r_1) = r_1^2 I_c(1)$$

with lengths rescaled on r_1 and the tip Mach number M_t replaced by $r_1 M_t$. Note that since the wavenumber k depends on M_t, the scaling will also affect the phase term in the integral, so that k is replaced by kr_1.

The acoustic integral I is now in a form which permits application of the method developed previously by Chapman [15] and extended by Carley [16]. Using this technique I_c can be calculated efficiently on a line of constant r—a "sideline" in propeller noise jargon—as a set of one-dimensional integrals. The problem of evaluating the two-dimensional integral of equation (7a) at single points over some region is replaced by that of evaluating $I_c(r_1)$ on sidelines and then integrating $I_c(r_1)h_n'$, a set of one-dimensional integrals the first of which can be performed very efficiently.

The first stage in the method is to transform the co-ordinates to centre on the sideline at r. Figure 2 shows the new co-ordinates in the source plane. The axial co-ordinate z remains unchanged while new co-ordinates (r_2, θ_2) are centred on the sideline. The relationship

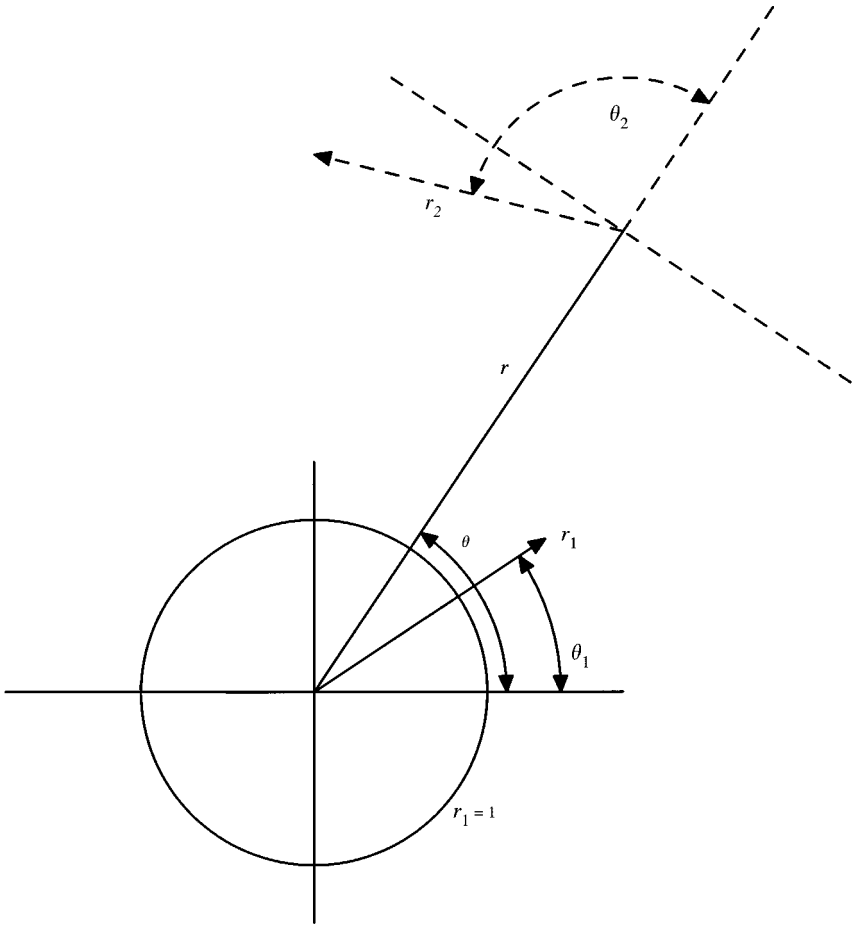

Figure 2. Sideline co-ordinate transformation.

between the old and new co-ordinate system is easily found:

$$r_1^2 = r^2 + r_2^2 + 2rr_2\cos\theta_2, \qquad \theta_1 = \tan^{-1}\frac{r_2\sin\theta_2}{r + r_2\cos\theta_2}, \tag{10a, b}$$

so that $r_1\,\mathrm{d}r_1\,\mathrm{d}\theta_1 = r_2\,\mathrm{d}r_2\,\mathrm{d}\theta_2$.

The transformed integral $I_c(1)$ is then

$$I_c(1) = \int_{\max(0,r-1)}^{r+1} \frac{\mathrm{e}^{\mathrm{j}(k\sigma + \mathrm{ej}k\sigma)}}{S^3}\left(S\sigma + \mathrm{j}\frac{M_\infty}{M_\mathrm{t}}\frac{z}{n}\right)J(r, r_2)r_2\,\mathrm{d}r_2, \tag{11}$$

$$J(r, r_2) = \frac{1}{2\pi}\int_{\theta_2^{(0)}}^{2\pi - \theta_2^{(0)}} \mathrm{e}^{-\mathrm{j}n\theta_1}\,\mathrm{d}\theta_2, \tag{12}$$

and $S = (\beta^2 r_2^2 + z^2)^{1/2}$,

$$\theta_2^{(0)} = \cos^{-1}\frac{(1 - r^2 - r_2^2)}{2rr_2}.$$

A recursion relation has been given for $J(r, r_2)$ when n is even [15] and finite and infinite series forms have also been derived [16] and are summarized in the appendix. In the case where n is odd, necessary both for propellers of odd blade number and for the calculation of noise radiated by unsteady sources on propellers of even blade number [17], the definition of $I_c(1)$ is modified slightly:

$$I_c(1) = r_1 \int_{\max(0, r-1)}^{r+1} \frac{e^{j(k\sigma e jk\sigma)}}{S^3} \left(S\sigma + j \frac{M_\infty}{M_t} \frac{z}{n} \right) J(r, r_2) r_2 \, dr_2. \tag{13}$$

$$J(r, r_2) = \frac{1}{2\pi} \int_{\theta_2} r_1^{-1} e^{-jn\theta_1} \, d\theta_2. \tag{14}$$

The inclusion of the term r_1^{-1} in the definition of $J(r, r_2)$ allows the use of the formulae previously derived [16] and given in Appendix A.

Thus, to conduct a parametric study of the effect of variations in the source distributions h_n, g_n and q_n at given operating conditions the integral $I_c(r_1)$ and the analogous loading noise integrals L_c and Q_c are precomputed over the desired region. This can be accomplished quite efficiently by computing all three together as most of the relevant quantities (S and σ for example) are the same in each case. To calculate the field for a given source distribution, the integration of equation (9) is then carried out. If only the directivity on a sideline is required, this can obviously be calculated much more quickly than for the whole field, but the procedure is identical.

3. THE STRUCTURE OF ROTATING SOUND FIELDS

The results presented later in this paper form a parametric study of the effect of variations in operating conditions and source distributions on the acoustic field of a rotating source. For comparison with previously published analytical results, particular geometry and loading distributions have been chosen (section 3.1) but the acoustic integrals for these sources are calculated exactly. The first paper to present exact results of the type shown here was that of Chapman [15], but a number of other authors have presented work which demonstrates important aspects of the behaviour of the acoustic field under various conditions. Most of these analyses have been limited to the far field and many of them have used asymptotic methods to derive simple formulae for the behaviour of the field while retaining much of the accuracy of the original integrals. It is known that in both the far field [10, 11] and the near field [12], the noise from subsonic rotors is dominated by the blade tip while for supersonic rotors it is controlled by the Mach radius, the point on the blade which approaches a field point at sonic velocity. In the case of a subsonic propeller, the relevant parameter is the radial source gradient near the blade tip and the source distributions chosen for the parametric study of section 4 reflect this.

It is noteworthy, however, that for both subsonic and supersonic propellers the field is divided by the sonic radius β/M_t, the point on the blade with unit helical Mach number. The nearfield analysis of Peake and Crighton [12] has demonstrated the existence of three distinct regions around a subsonic propeller, the near field $r < \beta/M_t$, the far field $r > \beta/M_t$ and a transition region of width order $n^{-2/3}$ around the sonic radius. This behaviour was also seen in the stationary disc results of Chapman [15] and the translating propeller results of Carley [16]. The field is divided by the sonic radius. If the whole propeller disc lies within this radius, $\beta/M_t > 1$, the acoustic energy spirals many times around the propeller axis before "tunnelling" into the far field which is very weak. If part of the propeller disc lies

more than about half an acoustic wavelength outside the Mach radius, it can radiate directly into the far field with no energy being lost in tunnelling through the transition region. This gives the very strong beaming pattern characteristic of supersonic rotors [18]. If the propeller tip is only slightly supersonic, it does not penetrate far into the transition region and there is no strong beaming. The results to be presented in section 4 will demonstrate these effects and the dependence of the field on the source distribution.

3.1. SOURCE EFFECTS

For comparison with the subsonic propeller asymptotic theory [10], a source distribution is chosen which has a particular radial dependence. It is known that in the far field, the blade tip dominates the noise and that the amplitude of the harmonic depends on a parameter v where the source strength $s(r_1)$ near the tip varies as

$$s \sim S(1 - r_1)^v$$

with S being a constant. For this reason, the source distributions to be used later are of the form

$$s = (v + 1)(v + 2)(1 + r_1)^v, \tag{15}$$

where the factor $(v + 1)(v + 2)$ normalizes the total area-weighted source strength,

$$\left| \int_0^1 s(r_1) r_1 \, \mathrm{d}r_1 \right| \equiv 1,$$

ensuring that variations in overall source strength do not mask the underlying acoustical effects. This means that, for example, the loading noise fields are compared on the basis of constant net thrust.

The effect of the parameter v is shown in Figures 3 and 4 which plot the integrand $I_c(r_1)s'(r_1)$ for a subsonic and a supersonic propeller respectively. In both cases, the observer is close to the propeller plane at $r = 2{\cdot}5$. In the subsonic case, $M_t = 0{\cdot}7$, $M_\infty = 0{\cdot}2$, shown in Figure 3, the tip dominance is clearly shown. A $v = 1$, the integrand is finite at the tip but at larger v the integrand disappears at the tip and its maximum is much smaller; the curve also encloses a much smaller area. In the supersonic rotor case, $M_t = 1{\cdot}05$, $M_\infty = 0{\cdot}8$, shown in Figure 4, the very different behaviour to be expected from the asymptotic theory [11] is evident. Increasing v has little effect on the area under the curve and the peaks in $I_c(r_1)s'(r_1)$ are all of the same order of magnitude, independent of v.

4. ACOUSTIC FIELDS

The acoustic integrals have been calculated for a number of different values of v for both thickness and loading noise. In the loading noise case, blade twist has been included by decomposing the blade forces into thrust and drag terms (section 4.2). The integrals have been calculated over the region $0 \leqslant r \leqslant 3$, $-3 \leqslant z \leqslant 3$ at a resolution which depends on the operating conditions. The shortest wavelength λ_{min} in the far field can be estimated from the propeller tip and flight Mach numbers:

$$\lambda_{min} \approx \frac{2\pi}{nM_t} \frac{1}{(1 - M_\infty)}$$

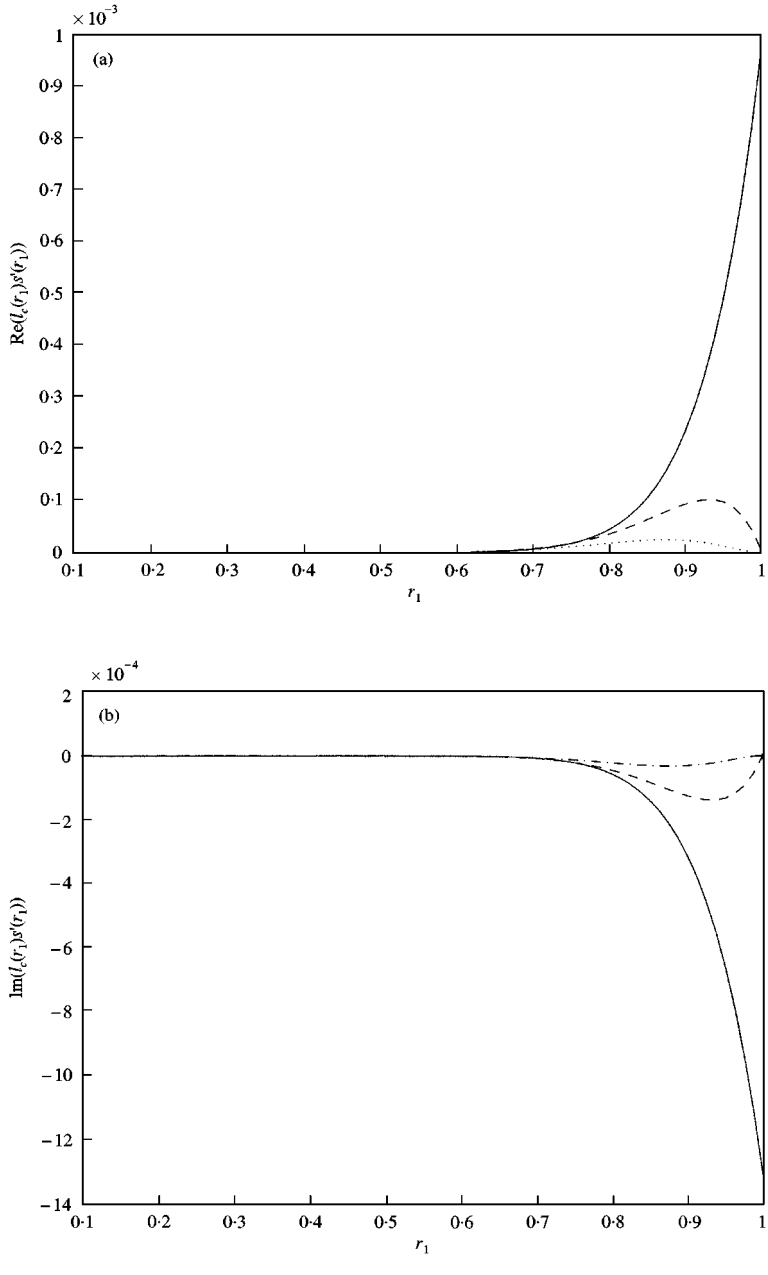

Figure 3. Integrand $I_c(r_1)s'(r_1)$ for $M_t = 0{\cdot}7$, $M_\infty = 0{\cdot}2$, $v = 1$: solid; $v = 2$: dashed; $v = 3$: dotted. a: real part; b: imaginary part.

and the resolution for the calculations is set at some fraction of this value (usually one-tenth). This represents an acceptable compromise between the need for adequate resolution of the field structure and the desire to minimize computation time. The calculated fields were spot-checked against the full two-dimensional integrals of equation (6), care being taken to check in regions of both high and low amplitudes.

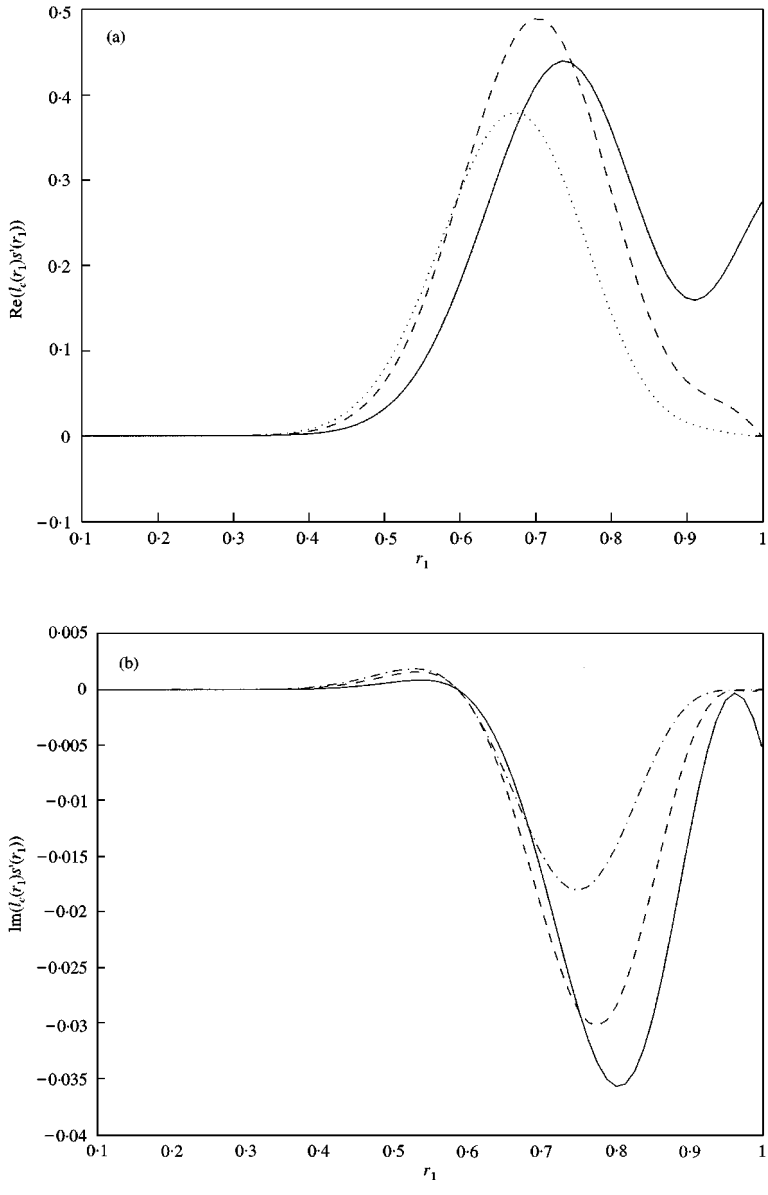

Figure 4. Integrand $I_c(r_1)s'(r_1)$ for $M_t = 1{\cdot}05$, $M_\infty = 0{\cdot}8$, $v = 1$: solid; $v = 2$: dashed; $v = 3$: dotted. a: real part; b: imaginary part.

From the large number of conditions for which calculations have been performed, two cases have been chosen as exemplary and the same calculations have been performed for each. The first is that of a subsonic propeller with $M_t = 0{\cdot}7$ and $M_\infty = 0{\cdot}2$, roughly take-off conditions. The second case is that of a supersonic propeller with $M_t = 1{\cdot}05$ and $M_\infty = 0{\cdot}8$. In both cases, the harmonic number $n = 16$. Between them, the results for these two operating conditions display most of the behaviour to be expected from the asymptotic theories.

4.1. THICKNESS NOISE

Figure 5 shows thickness noise fields for the subsonic propeller with $v = 1, 2, 3$. The same contour levels have been used in each case to make changes in the field more apparent. The obvious effect of increasing v, the source parameter, is that the region of the field enclosed by the contours shrinks rapidly. In each case, the field is strongest near the propeller plane and weakens near the axis of rotation; its absolute magnitude, however, depends on the on-blade source term and this is of concern in noise control and prediction. The effect of increasing v from 1 to 3 is to reduce the size of the lobe (defined by the outermost contours) by about half. Since, from equation (15), the integrated source strength is constant, this change can only be due to the change in the source structure and in particular to its variation near the blade tip, as predicted by asymptotic theories. This observed variation in the exact numerical results can be readily compared with that predicted by the analytical formulae derived from asymptotic analysis. The data are presented for conditions in which the blade tip is subsonic so that the theory should be accurate.

The relevant asymptotic theory is that of Parry and Crighton [10] which predicts that the farfield noise is tip-dominated and that the relevant parameter is the tip source gradient, controlled by v. In the notation of this paper and noting that, from equation (15) $S = (v + 1)(v + 2)$, the harmonic strength in the far field p_n varies as

$$p_n \sim \frac{1}{1 - M_\infty \cos\phi} \frac{(v+2)!}{(n \tanh\gamma)^{v+3/2}} e^{n(\tanh\gamma - \gamma)}, \tag{16}$$

where

$$\gamma = \operatorname{sech}^{-1}\left[\frac{M_t \sin\phi}{1 - M_\infty \cos\phi}\right],$$

and

$$\phi = \tan^{-1} r/z.$$

Figure 6 shows the value of p_n as a function of z at $r = 3$ for the values of v used in Figure 5. The lobe width for a given value of v can be found by tracing a horizontal line across the curves of Figure 6; the value of z at each intersection indicates the width of the lobe in Figure 6. For example, the value of p_n at $v = 3$, $z = 1$ is matched by the $v = 1, 2$ curves at $z = 2{\cdot}45$ and $1{\cdot}8$, respectively, indicating accurately the lobe width to be seen in Figure 6. The asymptotic theory accurately predicts the shrinking of the farfield lobe with increasing v as might be expected. It could also, of course, be used to predict the variation of any other feature of the field with the source parameter v.

In the case of a supersonic propeller, the behaviour is quite different; the blade tip is no longer dominant and the farfield amplitude is controlled by the Mach radius r^*, the point on the propeller blade which approaches a field point at sonic velocity:

$$r^* = \frac{(1 - M_\infty \cos\phi)}{M_t \sin\phi}.$$

In this case, the asymptotic theory [11] predicts a different variation in the farfield harmonic strength:

$$p_n \sim (v + 1)(v + 2) \frac{(1 - r^*)^v}{(1 - M_\infty \cos\phi)} \frac{r^*}{n}. \tag{17}$$

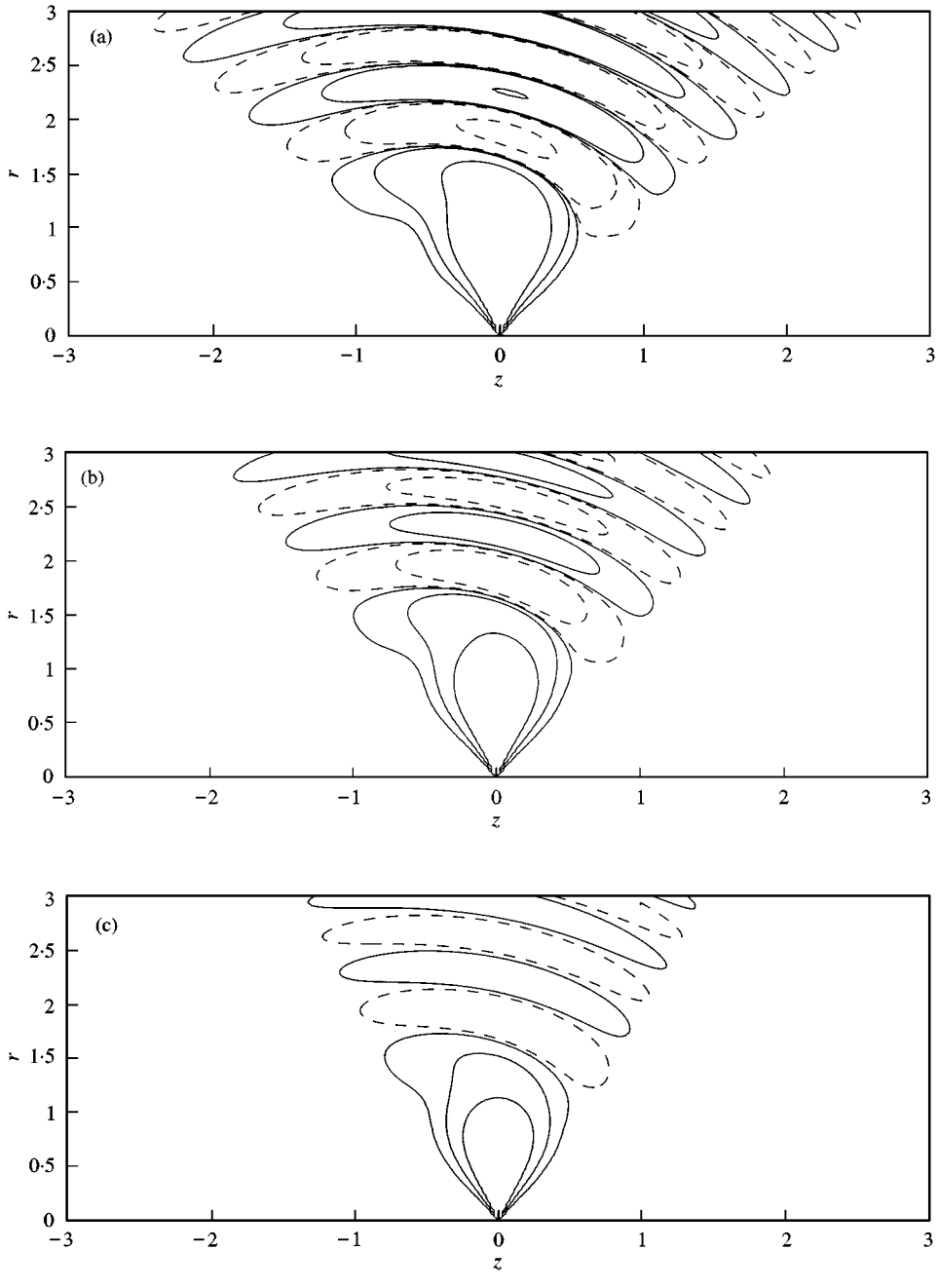

Figure 5. Thickness noise fields for $M_t = 0{\cdot}7$, $M_\infty = 0{\cdot}2$. (a) $v = 1$, contour levels $\pm 10^{-6}$, $\pm 10^{-5}$, $\pm 10^{-4}$; (b) $v = 2$, contour levels $\pm 10^{-6}$, $\pm 10^{-5}$, 10^{-4}; (c) $v = 3$, contour levels $\pm 10^{-6}$, 10^{-5}, 10^{-4}.

The directivity patterns in Figure 7 are characteristic of a supersonic rotor [15, 18, 19] with a strong beaming pattern in the rotor plane which has been stretched backwards by the axial motion [16]. If the Mach radius $r^* < 1$ the field is dominated by the source at that point, as in equation (17). This is true in the frontal lobe of the directivity and it will be noted

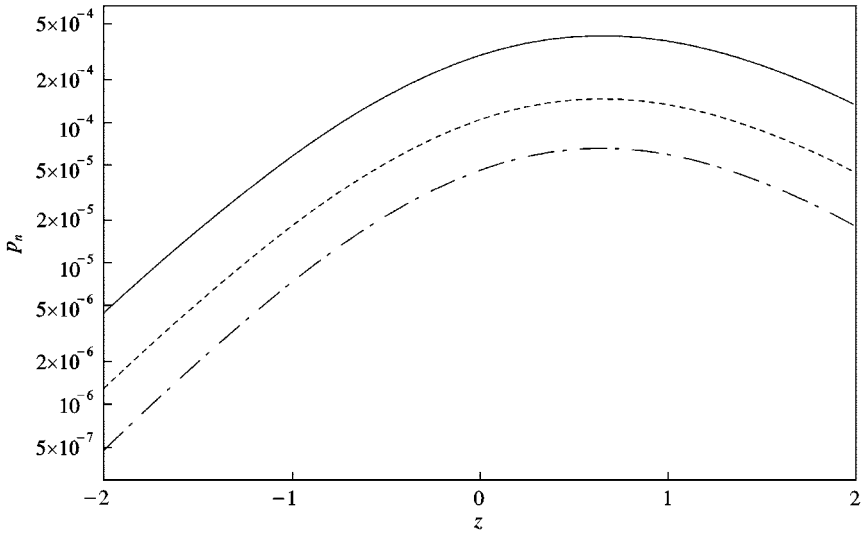

Figure 6. Asymptotic amplitude factor p_n for $M_t = 0{\cdot}7$, $M_\infty = 0{\cdot}2$, $v = 1$, solid; $v = 2$, dashed; $v = 3$, dash-dot.

that the size of the lobe shrinks much less rapidly with increasing v than in the subsonic rotor case. The operating conditions (M_∞, M_t) are identical in each of the three contour plots and so r^* does not change. The only difference between the three cases is now the value of $s(r^*)$. Figure 8 shows $s(r^*)$ for $0 \leqslant z \leqslant 3$ at $r = 3$. The change in $s(r^*)$ with z explains the weak variation in the main lobe size with changes in v. The source strength at r^* simply does not change much with v and its effect is quite small.

In summary, the thickness noise results are as would be expected from the farfield asymptotic theories, with the expected variation in field shape and strength as a function of the source characteristics.

4.2. LOADING NOISE

To demonstrate the application of the technique to the problem of calculating the loading noise field of a propeller, the case of a twisted blade with loading magnitude given by $s(r_1)$ will be considered. Figure 9 shows a blade section at some radial station, r_1. The force on the blade is f and it is aligned at a twist angle α to the flight direction. Any twist distribution $\alpha(r_1)$ could be used but here the blade section will be assumed to be aligned with the advance helix. Then $\alpha = \tan^{-1}(r_1 M_t / M_\infty)$ and the components of thrust and drag are

$$g_n = (v + 1)(v + 2)(1 - r_1)^v \frac{r_1 M_t}{M_h}, \tag{18a}$$

$$g_n = (v + 1)(v + 2)(1 - r_1)^v \frac{M_\infty}{M_h}, \tag{18b}$$

where $M_h = (r_1^2 M_t^2 + M_\infty^2)^{1/2}$, the section helical Mach number. A similar derivation can be found in the nearfield asymptotic analysis of Peake and Crighton [12]. It is re-emphasized

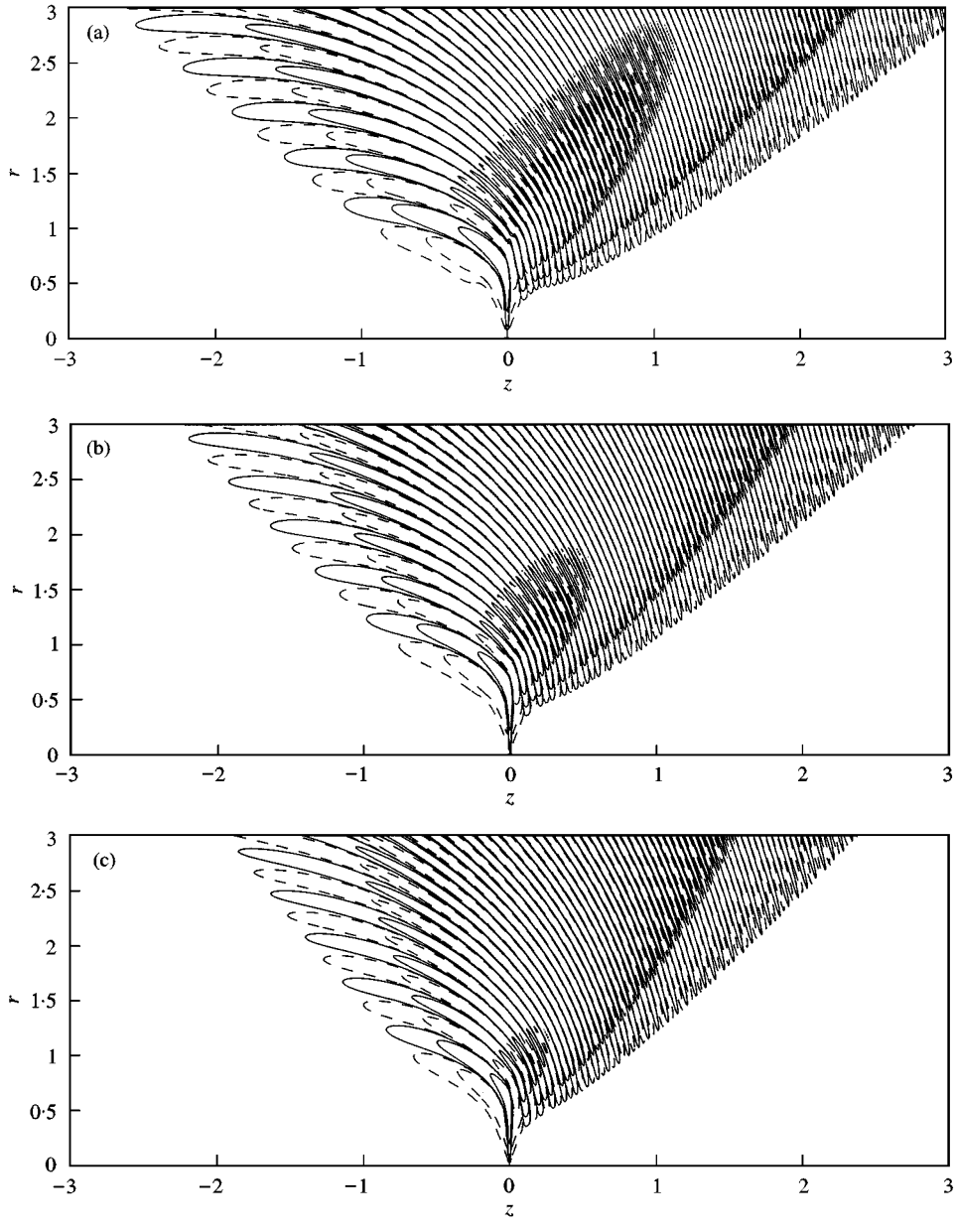

Figure 7. Thickness noise fields for $M_t = 1{\cdot}05$, $M_\infty = 0{\cdot}8$. (a) $v = 1$, contour levels $\pm 10^{-3}$, $\pm 10^{-2}$, $\pm 10^{-1}$; (b) $v = 2$, contour levels $\pm 10^{-3}$, $\pm 10^{-2}$, $\pm 10^{-1}$; (c) $v = 3$, contour levels $\pm 10^{-3}$; $\pm 10^{-2}$, $\pm 10^{-1}$.

that due to the normalization of the source term introduced in equation (15), the results presented here are all for propellers with equal total loading.

The acoustic integrals are calculated in the same manner as for the thickness noise. Figure 10 shows a section through the loading noise field for the subsonic propeller. As in the thickness noise case, the lobe in the radiated field shrinks rapidly with v. In Figure 11, showing sections perpendicular to the propeller axis at $z = 0{\cdot}1$, the "acoustic orange" of

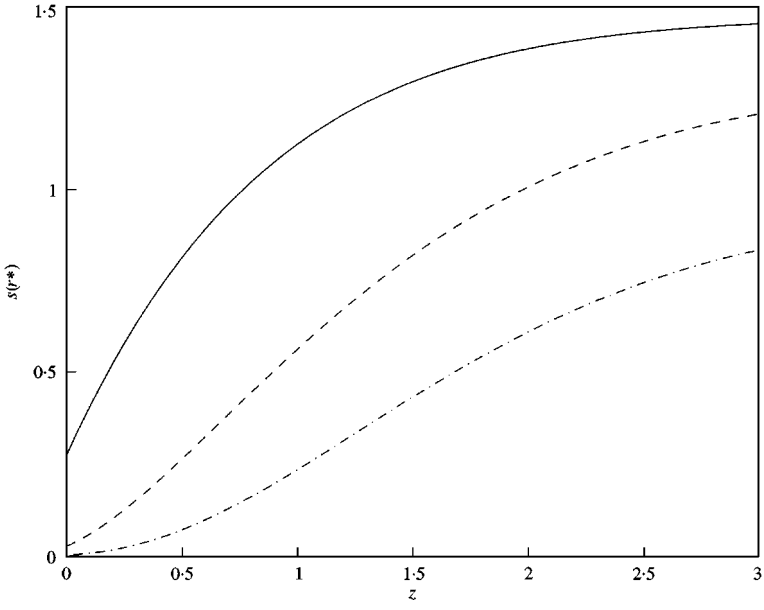

Figure 8. Source function $s(r^*)$ for $M_t = 1{\cdot}05$, $M_\infty = 0{\cdot}8$ as a function of z at $r = 3$; solid line, $v = 1$; dashed line, $v = 2$; dot-dashed line $v = 3$.

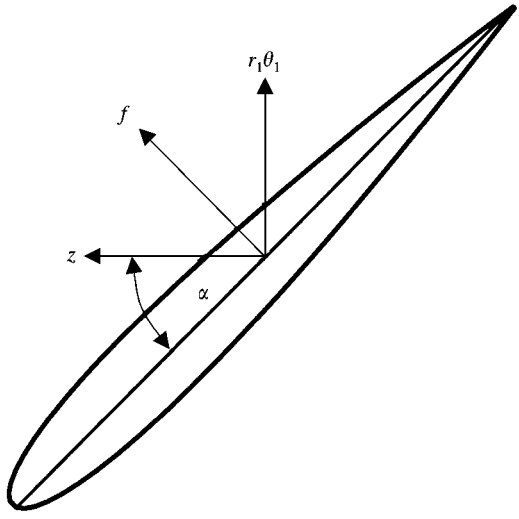

Figure 9. Blade section at twist angle α.

earlier work [15, 16] becomes apparent. The near field is made up of segments with almost straight boundaries which start to bend as the far field is reached. Acoustic energy spirals around the propeller axis many times before "tunnelling" into the far field where it radiates quite weakly. As might be expected by now, as v increases, the far field becomes much weaker with a faster decay around the sonic radius $\beta/M_t = 1{\cdot}4$. In the supersonic propeller

case shown in Figures 12 and 13, the field is quite different from the results presented in earlier work [16]. In that earlier work, a comparable result for an untwisted blade with $v = 0$ was published and the difference is in the transition across the disc boundary. In the case of pure thrust, with no decay near the tip, the pressure field is discontinuous with

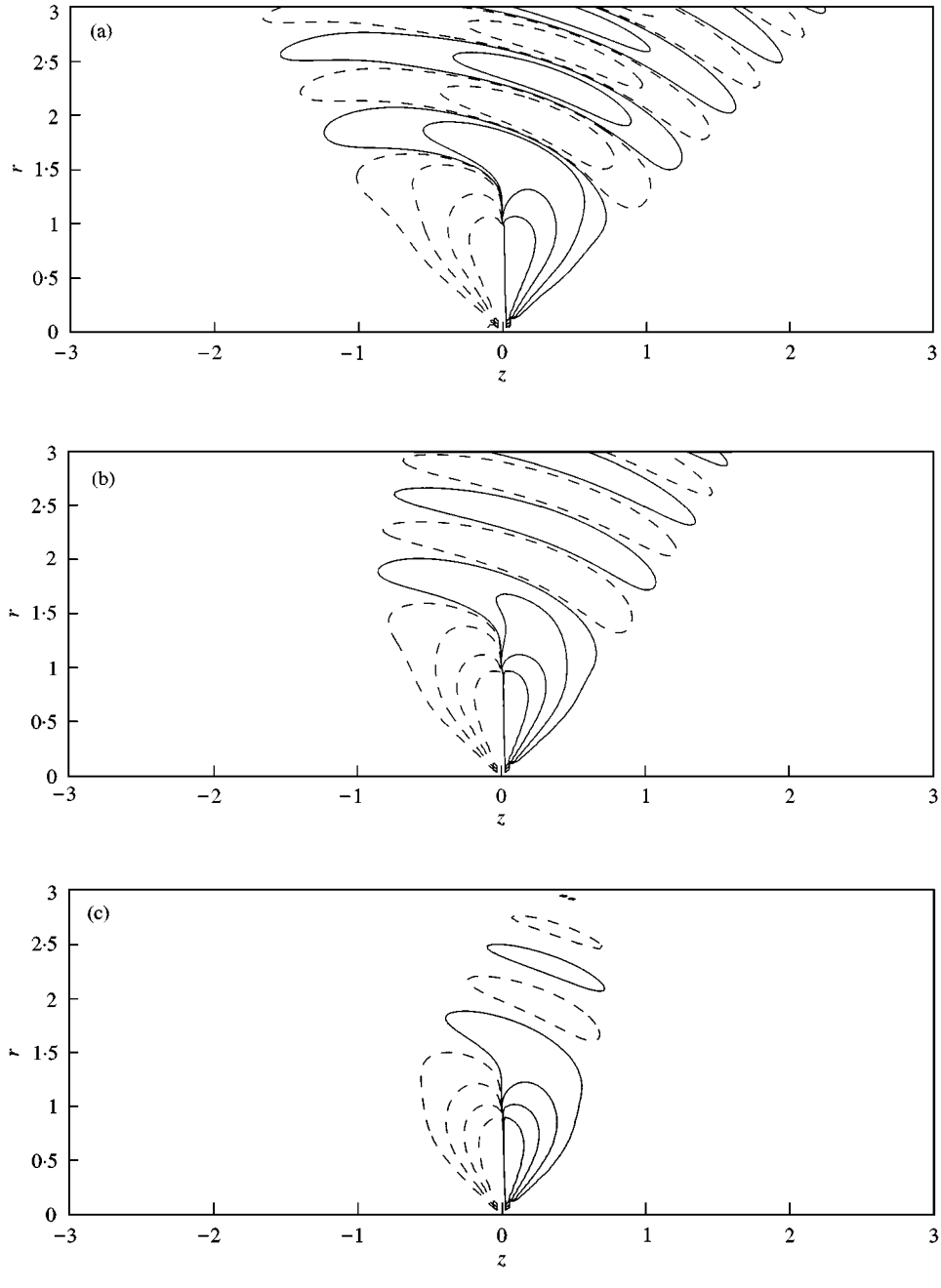

Figure 10. Loading noise fields for $M_t = 0{\cdot}7$, $M_\infty = 0{\cdot}2$, $\theta = 0$. (a) $v = 1$, contour levels $\pm 10^{-5}$, $\pm 10^{-4}$, $\pm 10^{-3}$; (b) $v = 2$, contour levels $\pm 10^{-5}$, $\pm 10^{-4}$, $\pm 10^{-3}$; (c) $v = 3$, contour levels $\pm 10^{-5}$, $\pm 10^{-4}$, $\pm 10^{-3}$.

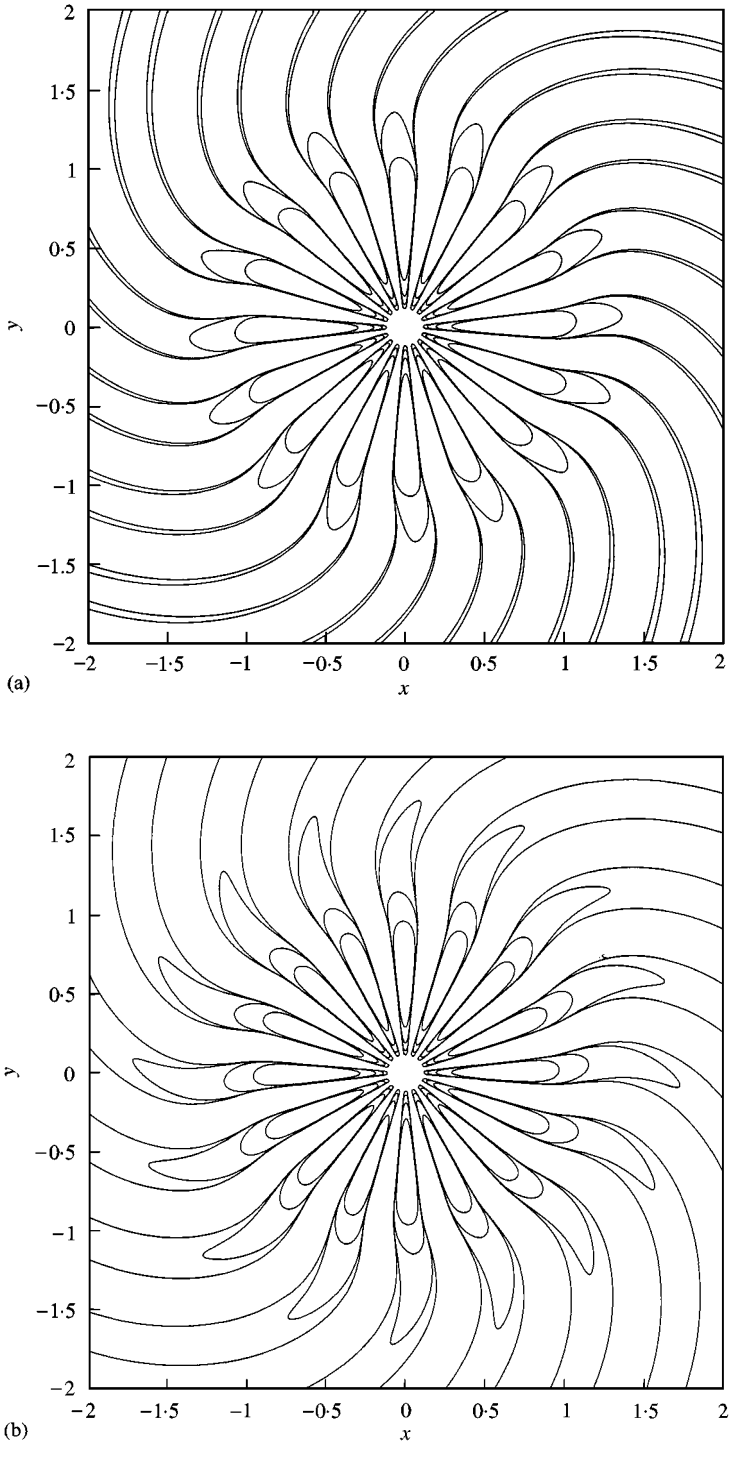

Figure 11. Loading noise fields for $M_t = 0{\cdot}7$, $M_\infty = 0{\cdot}2$, $z = 0{\cdot}1$. (a) $v = 1$, contour levels $\pm 10^{-5}$, $\pm 10^{-4}$, $\pm 10^{-3}$; (b) $v = 2$, contour levels 10^{-5}, 10^{-4}, 10^{-3}; (c) $v = 3$, contour levels 10^{-5}, 10^{-4}, 10^{-3}.

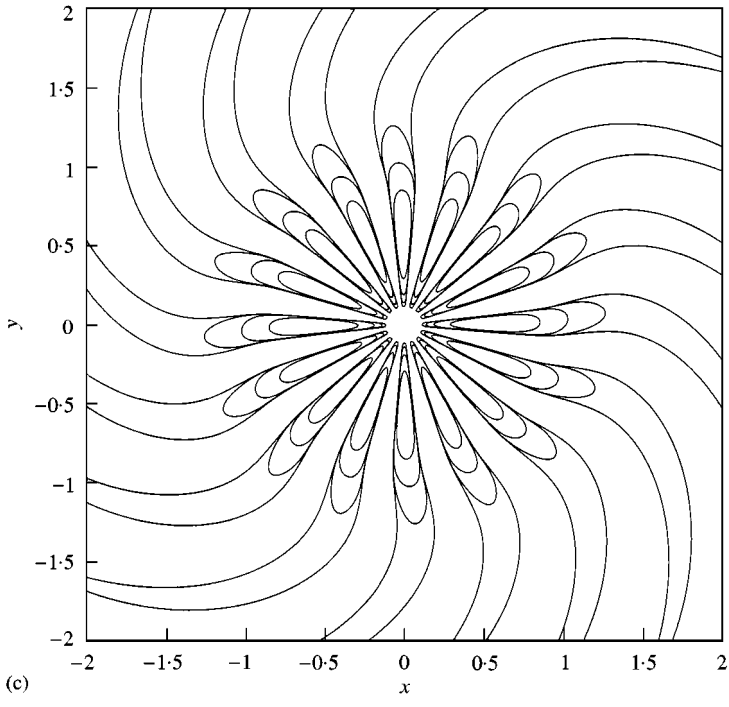

Figure 11. Continued

a jump on the $z = 0$ plane for $0 \leqslant r \leqslant 1$. In the results presented here, where the blade loading decays to zero at the tip, the pressure is continuous across $r = 1$. As this is a more realistic condition than the finite tip source assumed in the earlier studies of this type [15, 16], it is an important result to note while interpreting data of the type presented here. Even in the supersonic rotor case, where the asymptotic theory predicts that the blade tip loading is not the dominant factor, it can, indirectly, have an influence on the character of the field. As the far field is reached in the $z = 0{\cdot}1$ plots of Figure 13, the change in the noise amplitude with v is not very pronounced; the essential properties of the field are the same in each case.

In conclusion, the loading noise results show the same field structure as before [15, 16], with the important caveat that the inclusion of a decay in loading near the blade tip removes the abrupt change in pressure as the disc radius is crossed, an effect which is visible even in the supersonic loading cases where the blade tip is not normally considered important.

5. CONCLUSIONS

A method has been developed for the efficient, exact, numerical calculation of the acoustic field radiated by a spinning distribution of sources in axial motion. The method, which is quite general, has been applied to a study of propeller noise fields, concentrating on those parameters known from asymptotic theories to be important. The conclusions of the asymptotic theories and of previous, more restricted, studies of this type have been confirmed and the technique appears to be a useful addition to the methods available to

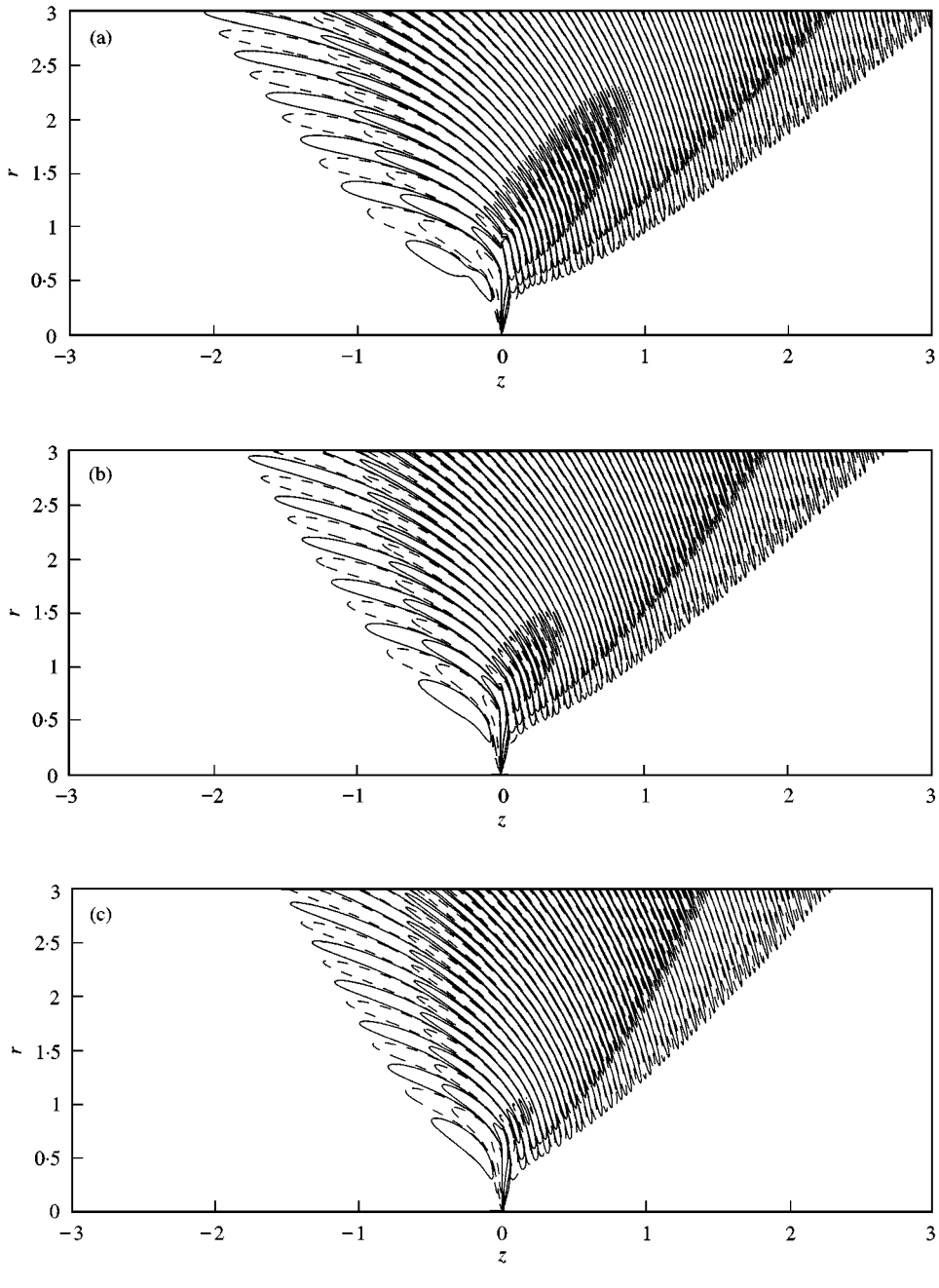

Figure 12. Loading noise fields for $M_t = 1{\cdot}05$, $M_\infty = 0{\cdot}8$, $\theta = 0$. (a) $v = 1$, contour levels $\pm 10^{-3}$, $\pm 10^{-2}$, $\pm 10^{-1}$; (b) $v = 2$, contour levels $\pm 10^{-3}$, $\pm 10^{-2}$, $\pm 10^{-1}$; (c) $v = 3$, contour levels $\pm 10^{-3}$, $\pm 10^{-2}$, $\pm 10^{-1}$.

researchers in propeller noise and should be a convenient method for industrial noise prediction. Finally, it should be noted that, being based on the calculation of noise along sidelines, the method is inherently parallel and transfers easily to multi-processor computers.

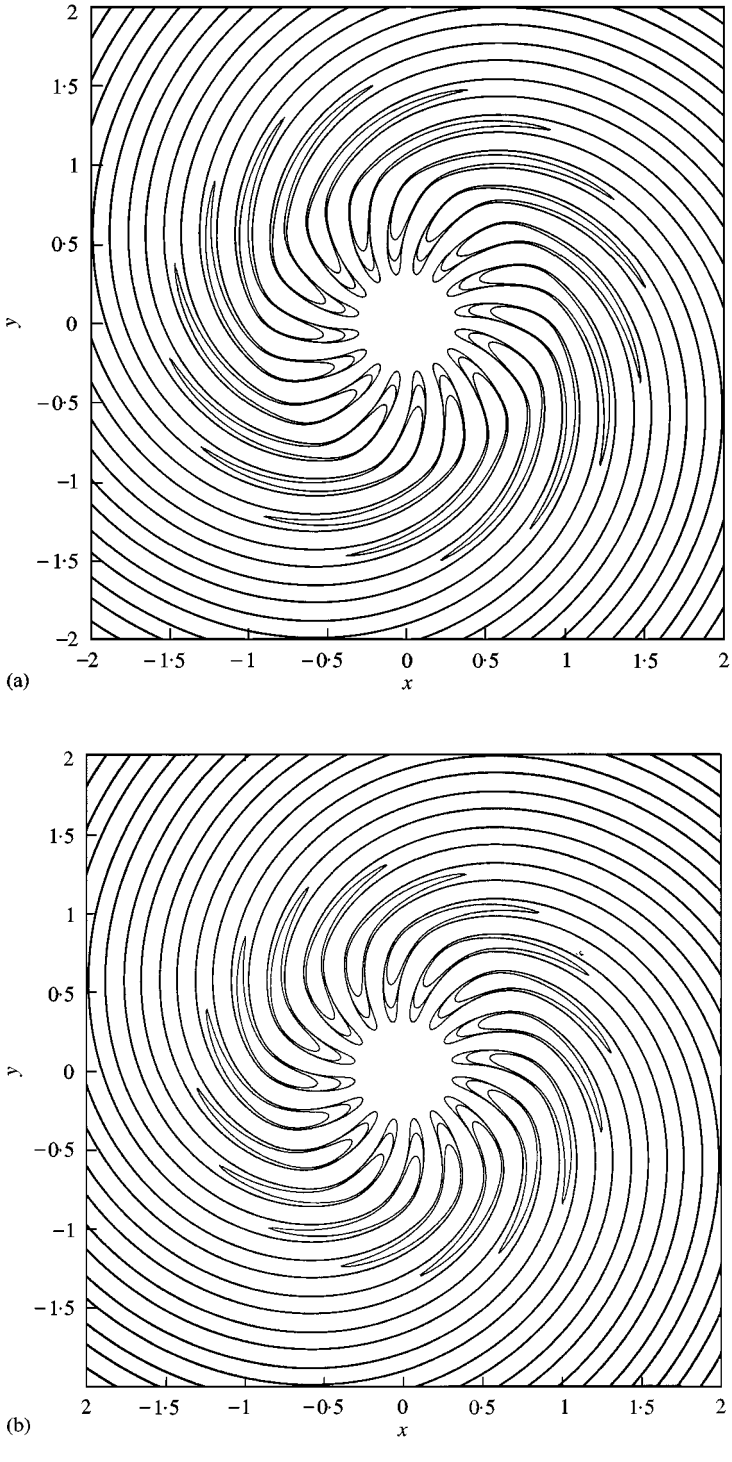

Figure 13. Loading noise fields for $M_t = 1{\cdot}05$, $M_\infty = 0{\cdot}8$, $z = 0{\cdot}1$. (a) $v = 1$, contour levels 10^{-2}, 10^{-1}, 10^{0}; (b) $v = 2$, contour levels 10^{-2}, $\pm\, 10^{-1}$, 10^{0}; (c) $v = 3$, contour levels 10^{-2}, 10^{-1}, 10^{0}.

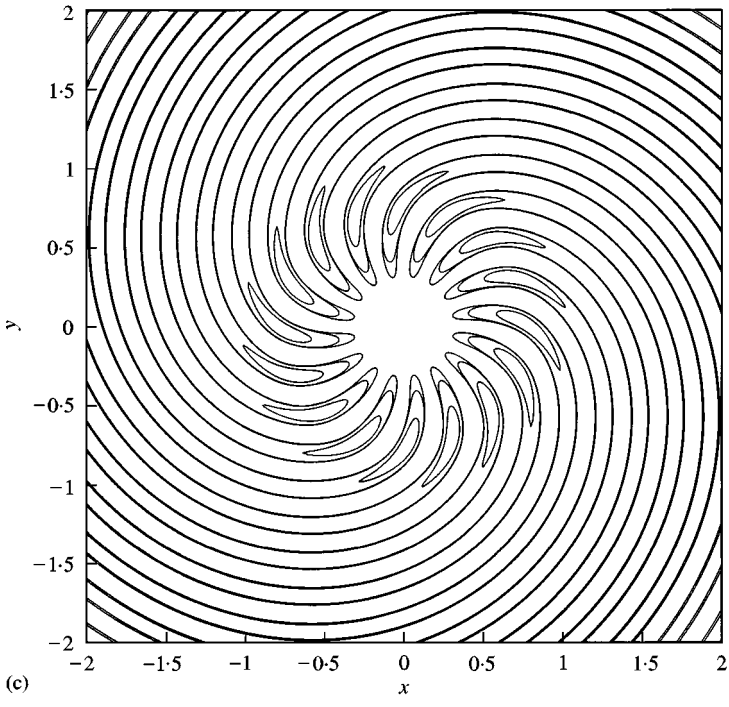

Figure 13. Continued

REFERENCES

1. E. J. H. LYNAM and H. A. WEBB 1919 *Reports and Memoranda* 624 *Aeronautical Research Committee*. The emission of sound by airscrews.
2. L. GUTIN 1948 *Technical Memorandum* 1195 *NACA*. On the sound field of a rotating propeller.
3. I. E. GARRICK and C. E. WATKINS 1953 *Report* 1198 *NACA*. A theoretical study of the effect of forward speed on the free-space sound-pressure field around propellers.
4. M. J. LIGHTHILL 1952 *Proceedings of the Royal Society of London A* **211**, 564–587. On sound generated aerodynamically: I General theory.
5. J. E. FFOWCS WILLIAMS and D. L. HAWKINGS 1969 *Philosophical Transactions of the Royal Society of London A* **264**, 321–342. Sound generation by turbulence and surfaces in arbitrary motion.
6. M. GOLDSTEIN 1974 *Journal of the Acoustical Society of America* **56**, 497–509. Unified approach to aerodynamic sound generation in the presence of solid boundaries.
7. F. FARASSAT 1981 *American Institute of Aeronautics and Astronautics Journal* **19**, 1122–1130. Linear acoustic formulas for calculation of rotating blade noise.
8. F. FARASSAT and K. S. BRENTNER 1998 *Proceedings of the 4th AIAA/CEAS Aeroacoustics Conference*. A study of supersonic surface sources—the Ffowcs Williams–Hawkings equation and the Kirchoff formula.
9. D. B. HANSON 1983 *American Institute of Aeronautics and Astronautics Journal* **21**, 881–888. Compressible helicoidal surface theory for propeller aerodynamics and noise.
10. A. B. PARRY and D. G. CRIGHTON 1989 *American Institute of Aeronautics and Astronautics Journal* **27**, 1184–1190. Asymptotic theory of propeller noise, Part I: subsonic single rotation propeller.
11. D. G. CRIGHTON and A. B. PARRY 1991 *American Institute of Aeronautics and Astronautics Journal* **29**, 2031–2037. Asymptotic theory of propeller noise. Part II: supersonic single rotation propeller.

12. N. PEAKE and D. G. CRIGHTON 1991 *Journal of Fluid Mechanics* **232**, 285–301. An asymptotic theory of near-field propeller acoustics.
13. C. J. CHAPMAN 1988 *Journal of Fluid Mechanics* **192**, 1–16. Shocks and singularities in the pressure field of a supersonically rotating propeller.
14. C. J. CHAPMAN 1990 *Proceedings of the Royal Society of London A* **431**, 157–167. The spiral Green function in acoustics and electromagnetism.
15. C. J. CHAPMAN 1993 *Proceedings of the Royal Society of London A* **440**, 257–271. The structure of rotating sound fields.
16. M. CARLEY 1999 *Journal of Sound and Vibration* **225**, 353–374. Sound radiation from propellers in forward flight.
17. S. E. WRIGHT 1969 *Journal of Sound and Vibration* **9**, 223–240. Sound radiation from a lifting rotor generated by asymmetric disk loading.
18. D. L. HAWKINGS and M. V. LOWSON 1974 *Journal of Sound and Vibration* **36**, 1–20. Theory of open supersonic rotor noise.
19. C. J. CHAPMAN 1992 *Proceedings of the Royal Society of London A* **436**, 511–526. The asymptotic theory of rapidly rotating sound fields.

APPENDIX A: FORMULAE FOR $J(r, r_2)$

In calculating the integrals I_c, L_c and Q_c, the function $J(r, r_2)$ is required. Formulae for this function have been derived previously [16] and are summarized here.

From Figure 2,

$$r_1 \mathrm{e}^{-j\theta_1} = \frac{r}{\mu}(\mu + r_2/r) \tag{A1}$$

and

$$r_1^2 = \frac{rr_2}{\mu}(\mu + r/r_2)(\mu + r_2/r) \tag{A2}$$

with $\mu \equiv \mathrm{e}^{\mathrm{j}\theta_2}$.

Two different cases must be considered, even n and odd n. First, for even n with $n = 2m$

$$J_{2m,0}(r, r_2) = \frac{1}{2\pi}\int_{\theta_2^{(0)}}^{2\pi - \theta_2^{(0)}} \mathrm{e}^{-\mathrm{j}2m\theta_1}\,\mathrm{d}\theta_2,$$

$$= t^{-m}\frac{1}{\mathrm{j}2\pi}\int_{\mu_0}^{\mu_0^*} \frac{(\mu + t)^m}{(\mu + \eta)^m}\frac{1}{\mu^{m+1}}\,\mathrm{d}\mu, \tag{A3}$$

where

$$\mu_0 = \mathrm{e}^{\mathrm{j}\theta_2^{(0)}}, \qquad \theta_2^{(0)} = \cos^{-1}\frac{(1 - r^2 - r_2^2)}{2rr_2},$$

$$t = r_2/r \quad \text{and} \quad \eta = r/r_2,$$

the notation of reference [16] having been adopted.

Secondly, when n is odd and equal to $2m + 1$, we introduce a term r_1^{-1} and

$$J_{2m+1,-1}(r, r_2) = r^{-1}t^{-1-m}\frac{1}{\mathrm{j}2\pi}\int_{\mu_0}^{\mu_0^*} \frac{(\mu + t)^m}{(\mu + \eta)^{m+1}}\frac{1}{\mu^{m+1}}\,\mathrm{d}\mu. \tag{A4}$$

These integrals can be expanded into partial fractions and calculated in exact closed form:

$$J_{2m,0} = -\frac{1}{\pi}\sum_{k=0}^{m}\binom{m}{k}(-t^2)^k\sum_{i=1}^{k+1}\binom{m+k-i}{m-1}(-t)^{1-i}\frac{\sin(1-i)\theta_2^{(0)}}{(1-i)} + \frac{1}{\pi}\sum_{k=0}^{m}\binom{m}{k}(-t^2)^k\sum_{i=1}^{m}\binom{m+k-i}{m-i}(1/r)^{1-i}\frac{\sin(1-i)\alpha}{(1-i)}, \tag{A5}$$

$$J_{2m+1,-1} = -\frac{r^{-1}}{\pi}\sum_{k=0}^{m}\binom{m}{k}(-t^2)^k\sum_{i=1}^{k+1}\binom{m+k-i+1}{m}(-t)^{1-i}\frac{\sin(1-i)\theta_2^{(0)}}{(1-i)} + \frac{r^{-1}}{\pi}\sum_{k=0}^{m}\binom{m}{k}(-t^2)^k\sum_{i=1}^{m+1}\binom{m+k-i+1}{m-i+1}(-r)^{1-i}\frac{\sin(1-i)\alpha}{(1-i)} \tag{A6}$$

with

$$\alpha = \tan^{-1}\frac{\sin\theta_2^{(0)}}{(\eta+\cos\theta_2^{(0)})},$$

For $i = 1$ in the summations,

$$\frac{\sin(1-i)\theta_2^{(0)}}{(1-i)} \quad \text{is replaced by } \theta_2^{(0)} - \pi$$

and

$$\frac{\sin(1-i)\alpha}{(1-i)} \quad \text{is replaced by } \begin{cases}\alpha, & t \leqslant 1,\\ \alpha-\pi, & t > 1.\end{cases}$$

When r is small, there are rounding errors due to incomplete cancellation of large powers of $t = r_2/r$. In this case, an infinite series expansion in $\eta = r/r_2$ is used:

$$J_{2m,0} = -\frac{1}{\pi}\sum_{i=0}^{\infty}\binom{m+i-1}{m-1}(-\eta)^i\sum_{k=0}^{m}\binom{m}{k}\frac{\sin(2m+i-k)\theta_2^{(0)}}{(2m+i-k)}\eta^k, \tag{A7}$$

$$J_{2m+1,-1} = -\frac{r^{-1}t^{-1}}{\pi}\sum_{i=0}^{\infty}\binom{m+i}{m}(-\eta)^i\sum_{k=0}^{m}\binom{m}{k}\frac{\sin(2m+i-k+1)\theta_2^{(0)}}{(2m+i-k+1)}\eta^k, \tag{A8}$$